THE JOURNAL OF BIOLOGICAL CHEMISTRY VOL. 287, NO. 15, pp. 11740–11750, April 6, 2012


# Assembly and Channel Opening of Outer Membrane Protein in Tripartite Drug Efflux Pumps of Gram-negative Bacteria*[S]

Received for publication, December 5, 2011, and in revised form, January 5, 2012 Published, JBC Papers in Press, February 3, 2012, DOI 10.1074/jbc.M111.329375

**Yongbin Xu**[‡1,2], **Arne Moeller**[§1,3], **So-Young Jun**[‡], **Minho Le**[¶], **Bo-Young Yoon**[‡], **Jin-Sik Kim**[‡], **Kangseok Lee**[¶4], **and Nam-Chul Ha**[‡5]

*From the* [‡]*Department of Manufacturing Pharmacy, College of Pharmacy and Research Institute for Drug Development, Pusan National University, Busan 609-735, Korea, the* [§]*National Resource for Automated Molecular Microscopy, The Scripps Research Institute, La Jolla, California 92037, and the* [¶]*School of Biological Sciences, Chung-Ang University, Seoul 156-756, Korea*

**Background:** *Pseudomonas aeruginosa* mainly achieves multidrug resistance by use of the MexAB-OprM pump.
**Results:** We determined the crystal structure of MexA. Electron microscopy work using MexA and OprM reveals that MexA makes a tip-to-tip interaction with OprM.
**Conclusion:** We suggest an assembly and channel opening model for the pump.
**Significance:** This study provides a better understanding of multidrug resistance in Gram-negative bacteria.

**Gram-negative bacteria are capable of expelling diverse xenobiotic substances from within the cell by use of three-component efflux pumps in which the energy-activated inner membrane transporter is connected to the outer membrane channel protein via the membrane fusion protein. In this work, we describe the crystal structure of the membrane fusion protein MexA from the *Pseudomonas aeruginosa* MexAB-OprM pump in the hexameric ring arrangement. Electron microscopy study on the chimeric complex of MexA and the outer membrane protein OprM reveals that MexA makes a tip-to-tip interaction with OprM, which suggests a docking model for MexA and OprM. This docking model agrees well with genetic results and depicts detailed interactions. Opening of the OprM channel is accompanied by the simultaneous exposure of a protein structure resembling a six-bladed cogwheel, which intermeshes with the complementary cogwheel structure in the MexA hexamer. Taken together, we suggest an assembly and channel opening model for the MexAB-OprM pump. This study provides a better understanding of multidrug resistance in Gram-negative bacteria.**

One mechanism of multidrug resistance in bacteria is enabled by the activity of efflux transporters that expel a diverse range of xenobiotics and antibiotics within the cell (1). In Gram-negative bacteria, the tripartite efflux pumps, which span the inner and outer membrane and the periplasmic space, translocate these diverse substances out of the cell (2). These efflux pumps are comprised of an inner membrane transporter, an outer membrane efflux protein (OEP),[6] and a membrane fusion protein (MFP) that links the two components in the periplasm (3).

In *Escherichia coli*, the AcrA-AcrB-TolC pump plays a central role in the multidrug resistance (3). The inner membrane transporter AcrB belongs to the resistance nodulation cell division (RND)-type transporter family, which utilizes the proton gradient across the inner membrane (4) to drive the process. AcrB forms a homotrimeric assembly and translocates diverse materials through the pore at the top of the periplasmic domain (5). The OEP TolC exhibits a homotrimeric assembly that includes the membrane-anchoring $\beta$-barrel domain and the cavity-forming $\alpha$-barrel domain, which is composed of six long $\alpha$-hairpin equivalents (6). In the absence of the other components, the TolC channel remains closed at the periplasmic end of the cylinder due to the interactions of adjacent $\alpha$-hairpins with salt bridges and hydrogen bond networks (6, 7).

The MFP AcrA is crucial for the functional assembly of the pump by bridging AcrB and TolC in the periplasmic space (8, 9), comprising the membrane proximal domain, $\beta$-barrel domain, lipoyl domain, and $\alpha$-hairpin domain (10, 11). The $\alpha$-hairpin domain is associated with the TolC $\alpha$-barrel domain (7, 12–14). Several independent studies recently converged onto a model, in which MFPs bind the cognate OEPs in stoichiometry six MFPs to the OEP trimer (14–19).

*Pseudomonas aeruginosa* is characterized by an innate multidrug resistance, which is significantly conferred by the RND-type efflux pump MexA-MexB-OprM (20). The MFP MexA is a lipoprotein that contains a palmitoyl chain linked on the N-terminal cysteine residue. The crystal structure of the MexA in the lipid moiety-free form exhibited the six- or seven-membered

* This work was supported by National Research Foundation of Korea Grant NRF-2009-0072268 (to N.-C. H.). This work made use of beamline NW3A at Photon Factory (Tsukuba, Japan).
*The atomic coordinates and structure factors (codes 4DK0 and 4DK1) have been deposited in the Protein Data Bank, Research Collaboratory for Structural Bioinformatics, Rutgers University, New Brunswick, NJ (http://www.rcsb.org/).*
*The three-dimensional density map of the A. actinomycetemcomitans MacA-MexAα hybrid structures has been deposited into the Electron Microscopy Data Bank (EMD-2044).*
[S] This article contains supplemental Tables S1 and S2 and Figs. S1–S4.
[1] Both authors contributed equally to this work.
[2] Present address: Dept. of Bioengineering, College of Life Science, Dalian Nationalities University, Dalian 116600, Liaoning, China.
[3] Supported by National Institutes of Health Roadmap Award P50 GM073197.
[4] To whom correspondence may be addressed. Tel.: 82-2-822-5241; Fax: 82-2-825-5026; E-mail: kangseok@cau.ac.kr.
[5] To whom correspondence may be addressed. Tel.: 82-51-510-2528; Fax: 82-51-513-6754; E-mail:hnc@pusan.ac.kr.

[6] The abbreviations used are: OEP, outer membrane efflux protein; MFP, membrane fusion protein; RND, resistance nodulation cell division.

twisted horseshoe assembly (21, 22), which does not directly explain the MexA assembly in the membrane bound state. However, cryo-microscopic results in the reconstructed membrane layer showed that the MexA forms a hexameric complex with a dimension of 13-nm height (15, 23, 24). This finding is consistent with the hexameric model of MexA proposed in the previous report (14).

The MacA-MacB-TolC pump exports macrolides and protein toxins in *E. coli* (25, 26), and the inner membrane component MacB is a member of the dimeric ATP-binding cassette transporter family (27, 28). The crystal structure of the MFP MacA revealed a funnel-like hexameric assembly, where the six α-hairpin domains from the hexamer pack to form a hollow cylinder (29). The functional importance of the hexameric funnel structure also has been demonstrated (29, 30). A chimeric protein containing the TolC α-barrel periplasmic end region formed a tight complex with MacA in an intermeshing cogwheel-to-cogwheel manner (30, 31). Results from the chimeric studies suggested that the assembly mechanism of AcrA and TolC share that of MacA and TolC (13, 14, 31). Recently, the crystal structure of CusB in complex with CusA, which are the components of an RND-type tripartite pump CusB-CusA-CusC, revealed that the MFP CusB assumes a funnel-like hexameric assembly upon interaction with the RND-type transporter (19). Nevertheless, the assembly mechanism for the RND-type efflux pump has been considered to remain unclear (16).

In this study, we determined the crystal structure of a chimeric protein containing the *P. aeruginosa* MexA α-hairpin domain. The electron microscopic study of the protein complex containing the MexA α-barrel and OprM α-barrel illustrates an intermeshing cogwheel-to-cogwheel interaction. Furthermore, the role of peptidoglycan in the channel opening of the outer membrane channel proteins is discussed.

## EXPERIMENTAL PROCEDURES

*Construction of Actinobacillus actinomycetemcomitans MacA-MexAα Hybrid and A. actinomycetemcomitans MacA-OprMα Hybrid Dimer*—To construct *A. actinomycetemcomitans* MacA-MexAα hybrid, DNA fragments encoding *A. actinomycetemcomitans* MacA residues 29–88, *P. aeruginosa* MexA residues 95–158, and *A. actinomycetemcomitans* MacA residues 181–394 were inserted into the NcoI and XhoI sites of the pPROEX-HTA (Invitrogen) vector, resulting in the vector pPRO-AaMacA-MexAα.

To construct the expression vector for *A. actinomycetemcomitans* MacA-OprMα hybrid dimer, DNA fragments encoding *A. actinomycetemcomitans* MacA residues 29–123, *P. aeruginosa* OprM residues 189–212, and *A. actinomycetemcomitans* MacA residues 148–394 without the stop codon were adjoined using the overlapping PCR technique, and then ligated into the NcoI and XhoI sites of pPROEX-HTA (Invitrogen), resulting in the vector pPRO-AaMacA-OprMα1-nostop. For the second *A. actinomycetemcomitans* MacA module, DNA fragments encoding *A. actinomycetemcomitans* MacA residues 29–123, *P. aeruginosa* OprM residues 396–419, and *A. actinomycetemcomitans* MacA residues 148–394 (including a stop codon) were adjoined to the XhoI and HindIII sites of the pPROEX-HTA vector. The second *A. actinomycetemcomitans* MacA module was inserted into the pPRO-AaMacA-OprMα1-nostop vector at the XhoI and HindIII sites, resulting in the vector pPRO-MacA-OprMα hybrid dimer.

*Overexpression and Purification of Recombinant Proteins*—*A. actinomycetemcomitans* MacA-MexAα hybrid and *A. actinomycetemcomitans* MacA-OprMα hybrid dimer proteins were overexpressed in *E. coli* and purified using the same method used for *A. actinomycetemcomitans* MacA as described previously (29).

*Electron Microscopy and Image Processing*—The sample was applied to a freshly plasma cleaned carbon-coated copper grid and allowed to adhere for 60 s before being blotted. Immediately after blotting, 3 μl of a 1% solution of uranyl formate was applied onto the grid and blotted off directly. This was repeated three times. Data were acquired using a Tecnai F20 Twin transmission electron microscope operating at 200 kV, using a dose of ~40 $e^-/Å^2$ and nominal underfocus ranging from 1.5 to 2.5 μm. At the specimen level, 1,440 high magnification images were automatically collected at a nominal magnification of 80,000× and pixel size 0.107 nm. All images were recorded with a Tietz F415 4k × 4k pixel CCD camera (15-μm pixel) utilizing Leginon data collection software (32). Experimental data were processed by the Appion software package (33), which interfaces with the Leginon database infrastructure. Automatic selection of 44,711 particles was conducted (34) from the micrographs and extracted at a box size of 400 pixels. XMIPP reference-free maximum likelihood alignment was applied to identify the best particles (35) from the selection. The final stack contained 2,244 particles that represented side views of the complex. The initial model was created by applying C6-symmetry on a manually selected two-dimensional average, which was formed using the XMIPP reference-free maximum likelihood alignment procedure (36). The three-dimensional reconstruction was carried out using the XMIPP reconstruction package (36). Resolution was assessed by calculating the Fourier shell correlation at a cut-off of 0.5, which provided a resolution of 24 Å. Automatic Docking was performed using the Chimera software package (37).

*Crystallization, Data Collection, and Structure Determination of A. actinomycetemcomitans MacA-MexAα*—*A. actinomycetemcomitans* MacA-MexAα hybrid (20 mg/ml) was crystallized in a precipitation solution containing 0.16 M calcium chloride dehydrate, 0.1 M HEPES sodium (pH 7.5), and 23.5% PEG 400 at 14 °C. The data set was collected on beamline 44 at Spring-8 with the CCD detector MX-225 (Marresearch) at −100 °C. The diffraction data were processed and scaled using the HKL2000 package (38). The resulting crystal belongs to the space group *P*321 with cell dimensions of $a = b = 151.7$ Å and $c = 216.9$ Å. Initial phases were determined using the molecular replacement package MOLREP (39) and the coordinates of a truncated version of the *A. actinomycetemcomitans* MacA structure at the α-hairpin tip region as a search model. Model building was performed using the program COOT (40), and model refinement was conducted using the programs PHENIX.REFINE (41) and REFMAC5 (39). Crystallographic data statistics are summarized in Table 1. All figures were prepared using PyMOL (42).

**TABLE 1**

**X-ray data collection and refinement statistics for *A. actinomycetemcomitans* MacA-MexAα hybrid**

The numbers in parentheses are statistics for the highest resolution shell. $R_{free}$ was calculated with 5% of the data set. r.m.s.d., root mean square deviation.

| | |
|---|---|
| **Data** | |
| Source | BL-NW3A at photon factory AR |
| Wavelength (Å) | 1.0000 |
| Resolution limit (Å) | 20–3.5 (3.56–3.5) |
| Space group | *P*321 |
| Unit cell (Å) | $a = b = 151.7$ and $c = 216.9$ Å; $\alpha = \beta = 90°$ and $\gamma = 120°$ |
| Reflections | |
| Unique | 33,690 |
| Redundancy | 6.6 (4.0) |
| $R_{sym}$ (%) | 14.6 (35.8) |
| Completeness (%) | 91.5 (95.0) |
| $I/\sigma$ | 12.7 (3.8) |
| **Refinement** | |
| Resolution range (Å) | 20.0–3.5 |
| *R* factor (%) | 31.4 |
| $R_{free}$ (%) | 36.8 |
| Average B value (Å$^2$) | 83.2 |
| r.m.s.d. for bonds (Å) | 0.025 |
| r.m.s.d. for angles | 2.973° |

*Refinement of A. actinomycetemcomitans MacA*—The crystallization, data collection, and structural determination of *A. actinomycetemcomitans* MacA were described previously (29, 43). To build the complete model for *A. actinomycetemcomitans* MacA, the membrane proximal domain from ZneB was fitted to the MAD-phasing electron density map of *A. actinomycetemcomitans* MacA. The residues located in the ZneB membrane proximal domain were substituted with those of *A. actinomycetemcomitans* MacA and subsequently refined using the program PHENIX.REFINE (41).

*Size Exclusion Chromatography*—To determine the molecular weight of the proteins in this study, size exclusion chromatography was performed at a flow rate of 0.5 ml/min on Superdex S-200 HR 10/30 (GE Healthcare) and equilibrated with 20 mM Tris buffer (pH 8.0) containing 150 mM NaCl.

*In Vitro Binding Assay Using CNBr-activated Resin*—The TolC α-barrel tip, OprM α-barrel tip, MacA-AcrAα hybrid, and *A. actinomycetemcomitans* MacA-MexAα hybrid all interacted. The MacA-AcrAα hybrid and *A. actinomycetemcomitans* MacA-MexAα hybrid-coupled resins were prepared using CNBr-activated resin (50 μg; GE-Healthcare) and MacA-AcrAα hybrid (1 mg) or *A. actinomycetemcomitans* MacA-MexAα hybrid (1 mg) according to the manufacturer's instructions. MacA-TolCα hybrid dimer (3 mg/ml) and/or MacA-OprMα hybrid dimer (3 mg/ml) were incubated with the coupled resin (20 μl) for 2 h at room temperature. Next, the resin was thoroughly washed with PBS and evaluated using SDS-PAGE, with Coomassie Blue used to stain the protein bands.

*Purification of Peptidoglycans*—Peptidoglycan from *E. coli* was purified according to the methods of Leduc *et al.* (44) and Marcyjaniak *et al.* (45) with modifications. Briefly, *E. coli* strain K12 was grown at 37 °C in LB medium and harvested at an $OD_{600}$ of ~0.9. The cell pellet was suspended in 10 ml of distilled water, mixed with an equal volume of 8% SDS, and incubated for 30 min at 100 °C. After standing at room temperature overnight, the sample was centrifuged at 30 °C for 30 min at 1,800 × *g* (13,000 rpm) in a high speed centrifuge (Hanil). The gel-type pellet was suspended in 1 ml of water and then washed by four cycles of resuspension and recentrifugation in distilled water to remove traces of SDS. Finally, it was resuspended in 0.5 ml of 10 mM Tris buffer (pH 7.5). The resulting insoluble material was treated with DNase at 37 °C for 30 min, after that with α-amylase at 37 °C for 16 h, and then with pronase at 50 °C for 16 h. The used enzymes were washed from the peptidoglycan solution by boiling and centrifugation. The purified peptidoglycans were finally resuspended in 0.5 ml of 10 mM Tris buffer (pH 7.5).

## RESULTS

*Crystal Structure of MexA α-Hairpin Domain*—The MexA in the crystal tends to form the twisted horseshoe assembly during the crystallization (21, 22). The hexameric MexA could be observed only when it anchors to the membrane and/or binds to OprM (15, 23, 24). To obtain the hexameric form of MexA, we initially attempted to determine the crystal structures of the complex of MexA and OprM. However, it was not straightforward due to the integral membrane protein OprM, and the low affinity between the two proteins in the presence of the detergent that stabilizes the membrane protein. To overcome the problem, we had to construct the forced hexamer of MexA using the chimeric approach reported previously (14, 31). This approach has been proven to be effective in representing the functional structure of α-hairpin domain of AcrA, a MexA homolog, *in vivo* and *in vitro* (14).

A chimeric protein containing a MexA α-hairpin domain with *A. actinomycetemcomitans* MacA was generated as a hexamerization framework because *A. actinomycetemcomitans* MacA has the highest propensity to form a hexamer in solution as compared with other MFPs (29). The MacA α-hairpin domain was substituted by the corresponding region of MexA and resulted in the chimeric protein (named *A. actinomycetemcomitans* MacA-MexAα hybrid in this study) that is intended to mimic the hexamerized MexA α-hairpin domains that are capable of binding to OprM (Fig. 1*A*). Because only α-hairpin domains of MFPs are involved in the binding to the cognate OEPs (17, 30), the MexA α-hairpin domain in the chimeric protein should be suitable for investigating the interaction with OprM.

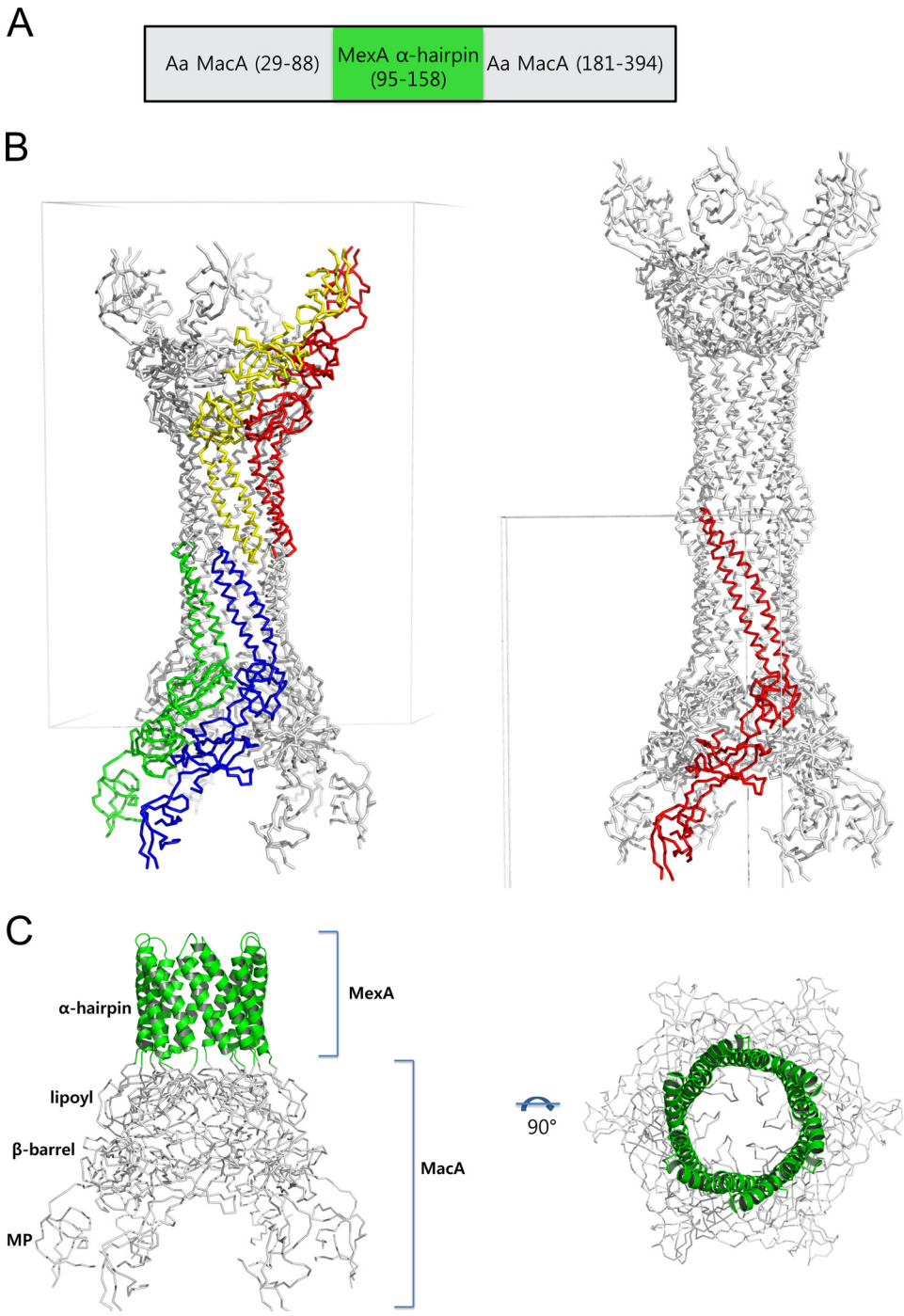


FIGURE 1. **Structure of *A. actinomycetemcomitans* MacA-MexAα hybrid.** *A*, schematic diagram of construction of *A. actinomycetemcomitans* MacA-MexAα hybrid. The α-hairpin domain of *A. actinomycetemcomitans* MacA (residues 89–180) is substituted with that of *P. aeruginosa* MexA (residues 95–158). *B*, crystal packing of *A. actinomycetemcomitans* MacA-MexAα hybrid, compared with that of *A. actinomycetemcomitans* MacA. *Left*, the asymmetric unit of *A. actinomycetemcomitans* MacA-MexAα hybrid is composed of a pair of dimeric units of the protein, which were colored *yellow*, *red*, *green*, or *blue*. The crystallographic 3-fold symmetry-related molecules are shown in *gray*. *Right*, the asymmetric unit of *A. actinomycetemcomitans* MacA is colored *red*, and the molecules generated by the crystallographic 6- and 2-fold are shown in *gray*. In both crystals, the hexameric units pack with tip-to-tip interactions. *C*, the hexameric structure of *A. actinomycetemcomitans* MacA-MexAα hybrid. This chimeric protein consists of an α-hairpin domain from *P. aeruginosa* MexA (*green*) and lipoyl, β-barrel, and membrane proximal (*MP*) domains, shown in *gray*, from *A. actinomycetemcomitans* MacA. The side view is displayed in the *left panel*, and the top view is shown in the *right panel*.

The chimeric protein *A. actinomycetemcomitans* MacA-MexAα hybrid was purified and crystallized to analyze the structure of the α-hairpin domain of MexA. The hexagonally shaped crystals were obtained and x-ray diffracted to a resolution of 3.5 Å. To build the complete model for the chimeric protein, we refined the crystal structure of *A. actinomycetemcomitans* MacA, whose experimental electron density and partial model were described previously (Fig. 1*B*, *right*) (29). Because the length of the α-hairpin of MexA is shorter than that of MacA, the end portion of the α-hairpin of *A. actinomycetemcomitans* MacA was cut to make a searching model for the molecular replacement approach (Fig. 1*B*, *left*).

The overall crystal packing of *A. actinomycetemcomitans* MacA-MexAα hybrid was similar to that of *A. actinomycetemcomitans* MacA, albeit a different space group (Fig. 1*C*). The six α-hairpin domains from the six protomers were packed side-by-side to make an α-barrel with a central hollow, as observed in the *A. actinomycetemcomitans* MacA crystal (Fig. 1*D*). When compared with α-hairpin domains from the full-length MexA structure (21, 22), any significant conformational change was not observed (supplemental Fig. S1). The end of the α-barrel was slightly flared because the first α-helices of the α-hairpins is twisted outward by ~60° at the tip region, exposing a six-bladed cogwheel (supplemental Fig. S2). The cogwheels of the chimeric protein intermeshed with the α-barrel from the neighboring molecules in the crystal (Fig. 1*C*, *left*). This crystal structure illustrates the propensity for hexameric cylinder formation in the α-hairpin of MexA, suggesting that MexA can form a funnel-like hexamer when the MexA is anchored to the membrane or binds to MexB or OprM.

*MexA α-Barrel Domain Interacts with OprM α-Barrel Tip Region*—To examine whether or not the MexA α-hairpin domain is capable of interacting with the α-barrel tip region of the cognate OEP OprM, as observed with AcrA and TolC, we constructed a chimeric protein containing the OprM α-barrel tip region based on the hexameric protein *A. actinomycetemcomitans* MacA, as used in construction of the TolC α-barrel tip region in the previous reports (14, 31). The OprM monomer consists largely of two repeats, which contain one α-hairpin at the α-barrel tip region such as TolC, whereas *A. actinomycetemcomitans* MacA has only one α-hairpin per monomer. To mimic the α-barrel tip region of OprM, two *A. actinomycetemcomitans* MacA protomers were fused in tandem and each of the *A. actinomycetemcomitans* MacA residues 124–147 were replaced with corresponding OprM residues, 188–212 (in repeat 1) or 396–419 (in repeat 2) (Fig. 2*A*). We designated the chimeric protein as *A. actinomycetemcomitans* MacA-OprMα hybrid dimer and generated a model based on the crystal structure of *A. actinomycetemcomitans* MacA (29), whose structure was refined in this study. The overall structure of the model for the chimeric protein was expected to be similar to *A. actinomycetemcomitans* MacA, to include the feature that the central channel is wide open in the OprM residue tip region (Fig. 2*B*). This open conformation is distinguished from the closed conformation observed in the crystal structure of the full-length OprM (Fig. 2*C*) (46).

This chimeric protein containing the OprM α-barrel tip region (*A. actinomycetemcomitans* MacA-OprMα hybrid dimer) exhibited a strong affinity to another chimeric protein containing MexA α-hairpin on a size exclusion chromatographic column (Fig. 3*A*), as observed in a study of *E. coli* AcrA and TolC (14). Interestingly, the *E. coli* TolC α-barrel tip-containing protein, referred to as *A. actinomycetemcomitans* MacA-TolCα hybrid dimer in the previous report (14), demonstrated a strong affinity to the MexA α-hairpin-containing protein and vice versa (Fig. 3*B*). This result indicates that *E. coli* AcrA and *P. aeruginosa* MexA share common structural motifs in TolC binding, which is consistent with a previous observation that a chimeric AcrA containing the MexA α-hairpin domain was as functional as the wild type AcrA *in vivo* (17).

It was reported previously that the stoichiometry of the MexA-OprM complex in a reconstituted membrane bilayer shows strong pH dependence (15). To examine the pH dependence of the MexA-OprM complex formation under detergent-free condition, we carried out the *in vitro* binding assay. The MacA-OprMα hybrid dimer protein was coupled to agarose resin, and then the MacA-MexAα hybrid protein was incubated at various pH values. After washing, the binding was monitored in Coomassie Blue-stained SDS-polyacrylamide gel (supplemental Fig. S4). The result implied that the binding of the MexA α-hairpin domain to the OprM α-barrel tip is not dependent on the external pH. We think that the protein-protein interaction may be interfered at a certain pH range by the detergent molecules used in a reconstituted membrane layer.

*Structure of OprM and MexA Complex, Visualized by Electron Microscopy*—To depict the binding interface between OprM and MexA, we carried out electron microscopic studies on the protein complex composed of the two chimeric proteins containing the OprM α-barrel tips and MexA α-hairpins. The hexagonal shape from the top view and indications of bridging from the side view were easily identified in the raw images (Fig. 4*A*). A projection-matching approach using side views of the negatively stained complex resulted in a three-dimensional density map at 24 Å resolution (Fourier shell correlation = 0.5). Two-dimensional class averages indicate greater flexibility at one of the two ends of the complex (Fig. 4*A*, *arrows*). In the resulting three-dimensional electron density maps, this flexibility is represented by additional masses at one of the two ends. In previous reports, similar electron microscopic analyses were done with the TolC α-barrel tip and MacA (31), and the TolC α-barrel tip and AcrA α-hairpin (14).

Compared with previous results (14, 31), the three-dimensional electron density map in this study demonstrated improved detail. The map displayed a characteristic hexagonal dumbbell-like structure with six spikes at both ends. However, the spikes were interlinked at only one end (Fig. 4*B*). A hexagonal cylindrical shape with a slight bulge was at the middle region of the dumbbell-like structure. A central channel of varying diameter with funnel-like openings on both ends threads through the complex.

*Docking of Atomic Models*—To gain more structural details of the MexA-OprM complexes, we docked the atomic models to the electron density map. Given the crystal structure of the chimeric protein containing the MexA α-hairpin (*A. actinomycetemcomitans* MacA-MexAα; Fig. 1*C*) and the atomic model of the chimeric *A. actinomycetemcomitans* MacA protein containing the OprM α-barrel tips (*A. actinomycetemcomitans* MacA-OprMα hybrid dimer; Fig. 2*B*), we first generated the complex model of the two structures in the intermeshing cogwheel-to-cogwheel manner. The atomic models were well fitted to the density, but only when the two six-bladed cogwheels intermeshed. The configurations of the atomic models were refined using a three-dimensional cross-correlation function (Fig. 5*A*). The intermeshing α-barrels from the two proteins were fitted to the central hex-cylindrical electron density map, and the slight bulge at the middle region (about one-third from the bottom; Fig. 4, *B*, *panel i*) of the HEX cylinder from the bottom in the electron density map perfectly matched the bind-

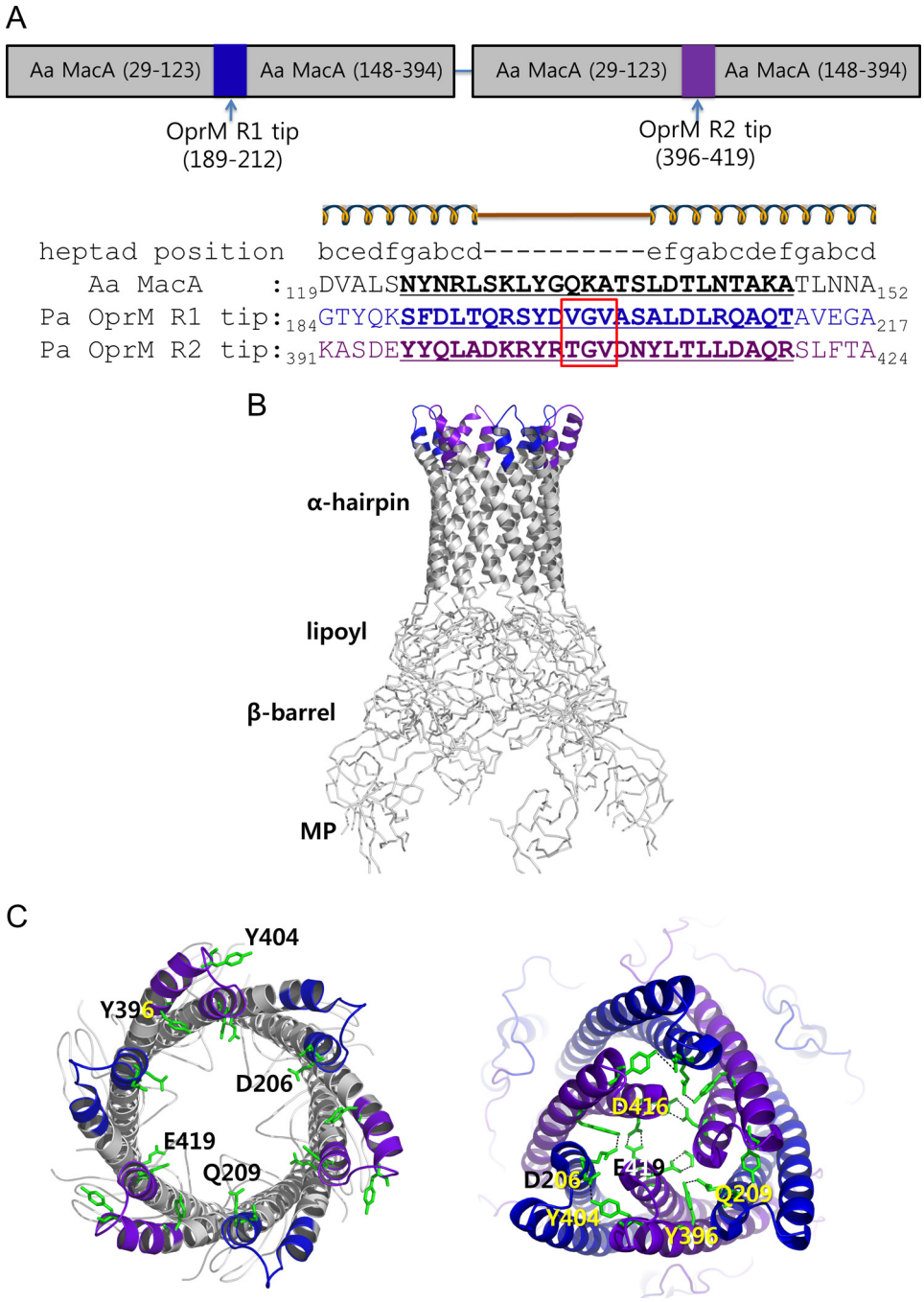


FIGURE 2. **Construction and structural models of *A. actinomycetemcomitans* MacA-OprMα hybrid dimer.** *A*, schematic diagram of construction of *A. actinomycetemcomitans* MacA-OprMα hybrid dimer. Two units of *A. actinomycetemcomitans* MacA are linked, and each *A. actinomycetemcomitans* MacA unit contains either the OprM α-hairpin tip region in repeat 1 (residues 189–212) or the tip region in repeat 2 (residues 396–419) instead of the corresponding region of *A. actinomycetemcomitans* MacA α-hairpin tip (residues 124–147). The amino acid sequence and the heptad positions are shown in the *bottom panel*. The *red box* indicates the conserved (V/T)GV motifs. *B*, molecular modeling of the chimeric protein *A. actinomycetemcomitans* MacA-OprMα hybrid dimer. The amino acids derived from OprM α-barrel tip regions are colored *blue* for repeat 1 and *purplish blue* for repeat 2. *C*, Top views of the chimeric protein of the *A. actinomycetemcomitans* MacA-OprMα hybrid dimer (*left*) and the crystal structure of OprM in the closed state (*right*). The channel of the chimeric protein is wide open at the OprM tip region. The residues involved in channel closing are shown in the stick representations. *MP*, membrane proximal.

ing interface between OprM and MexA. The bulge region may display the slightly flared ends of each α-barrel of the proteins, and the position of the bulge reflects the length difference of the α-hairpins because MacA α-hairpins are about two times longer than MexA α-hairpins.

The lipoyl and β-barrel domains were well suited to the spreading region in the electron density map, and the membrane proximal domains were strikingly fitted to the six spikes protruding from each end. We were able to unambiguously identify which side contained the OprM tip despite the structural similarity between the two chimeric proteins because only the *A. actinomycetemcomitans* MacA-OprMα hybrid dimer containing the OprM tip region had the linker at the membrane proximal domains between the two MacA units. As a final step

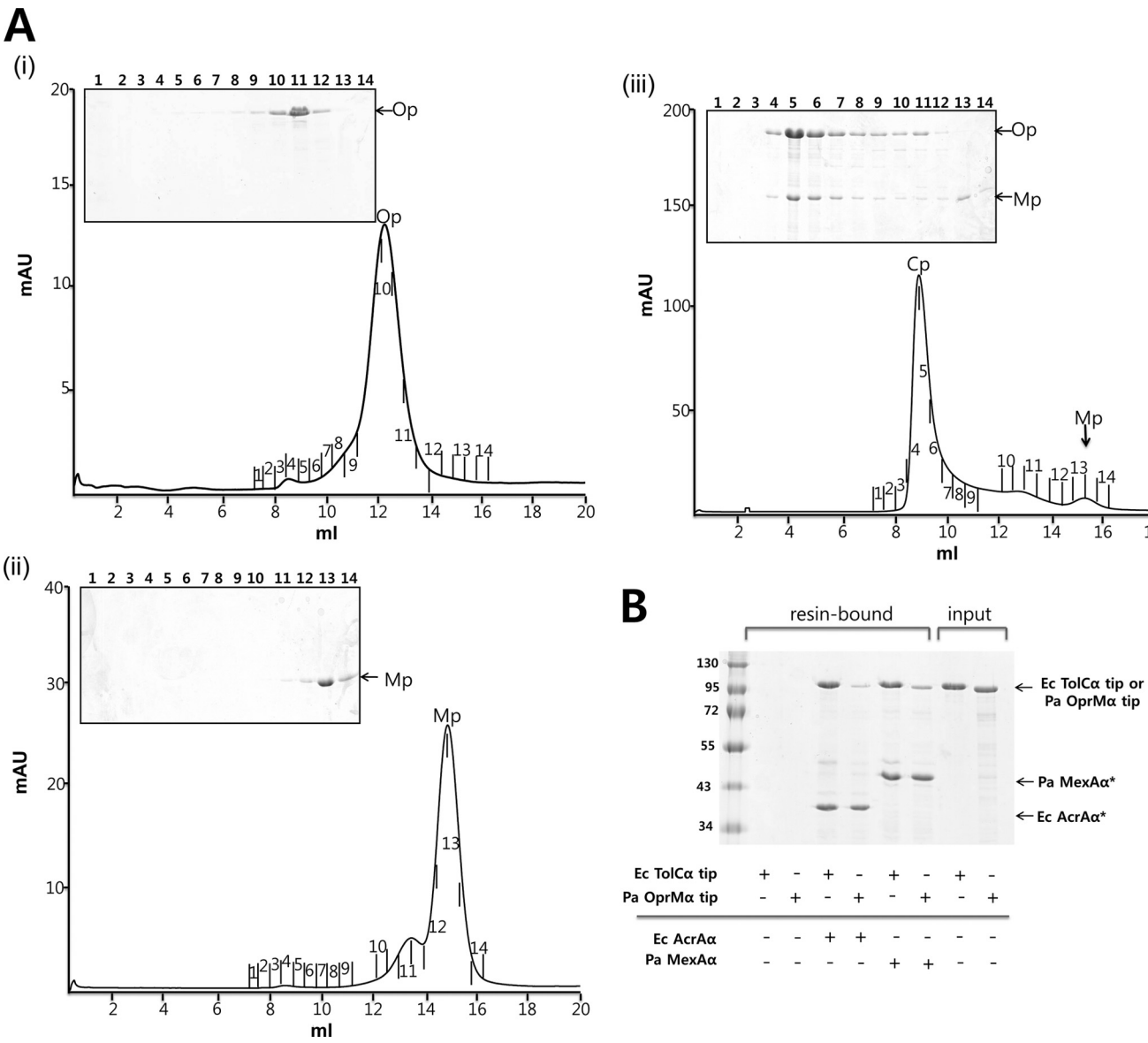


FIGURE 3. **Binding between MexA $\alpha$-hairpin and OprM $\alpha$-barrel tip regions.** *A*, the physical interaction between the OprM $\alpha$-barrel tip and the MexA $\alpha$-barrel tip regions as revealed by size exclusion chromatography using SDS-PAGE analysis. *i*, *A. actinomycetemcomitans* MacA-OprM$\alpha$ hybrid dimer protein (*Op*) alone. The result indicates that this protein forms a funnel-like structure as the elution volume is identical to hexameric *A. actinomycetemcomitans* MacA (data not shown). *ii*, *A. actinomycetemcomitans* MacA-MexA$\alpha$ hybrid protein (*Mp*) alone. The profile indicates that the protein is eluted as a monomer. *iii*, mixture of *A. actinomycetemcomitans* MacA-OprM$\alpha$ hybrid dimer and *A. actinomycetemcomitans* MacA-MexA$\alpha$ hybrid proteins. The peaks in the chromatogram indicate the complex (*Cp*), *A. actinomycetemcomitans* MacA-MexA$\alpha$ hybrid (*Mp*), and MacA-OprM$\alpha$ hybrid dimer (*Op*). According to the standard calibration curve for the size exclusion chromatographic column, MacA-OprM$\alpha$ hybrid dimer, *A. actinomycetemcomitans* MacA-MexA$\alpha$ hybrid, and the complex was calculated as 120, 61, and 670 kDa, respectively. *B*, the interaction of *P. aeruginosa* OprM $\alpha$-barrel tip or *E. coli* TolC $\alpha$-barrel tip with the $\alpha$-hairpin domains of MexA or AcrA. MacA-AcrA$\alpha$ hybrid that contains AcrA $\alpha$-hairpin domain (Ec AcrA$\alpha$) (14) or MacA-MexA$\alpha$ hybrid (Pa MexA$\alpha$) was covalently linked to agarose using CNBr-activated resin (50 $\mu$g; GE Healthcare) according to the manufacturer's instructions. Then, MacA-TolC$\alpha$ hybrid dimer protein (Ec TolC$\alpha$ tip; 1 mg) or MacA-OprM$\alpha$ hybrid dimer protein (Pa OprM$\alpha$ tip; 1 mg) was incubated with the agarose resin for 2 h at 4 °C, followed by thorough washing with PBS, and then application by SDS-PAGE. The *asterisk* indicates that the proteins were liberated partially from the resin by denaturation, even though the proteins were covalently attached to the resin, due to the multimeric structure of the proteins. Because a part of the MacA-OprM$\alpha$ hybrid dimer protein did not form the hexameric structure (*i*), the amount of the bound protein is relatively small compared with the MacA-TolC$\alpha$ hybrid dimer protein. However, the bindings of the protein to AcrA $\alpha$-barrel and MexA $\alpha$-barrel are strong and specific because the MacA-OprM$\alpha$ hybrid dimer protein is not bound to the resin in the absence of the bait proteins.

in building the model, the orientation of the side chains in the OprM and MexA $\alpha$-barrel tips were adjusted by molecular dynamics using CNS (Fig. 5*B*) (47).

In this complex model of OprM and MexA $\alpha$-barrel tips, the conserved amino acids, Arg-119, Leu-123, and Ser-130, of MexA contributed to OprM $\alpha$-barrel tip binding. This observation was consistent with previous reports that demonstrated the role of the OEP in binding and the functional importance of the three conserved residues (13, 14, 29–31). Arg-119 and Leu-123 were located at the end of the first $\alpha$-helical region of the $\alpha$-hairpin facing the right side of the cogwheel, whereas Ser-130 was located in the loop between the two $\alpha$-helices facing the opposite side of the cogwheel (Fig. 5*B*). The long aliphatic chain of Arg-119 occupied the empty space between the convex tip of

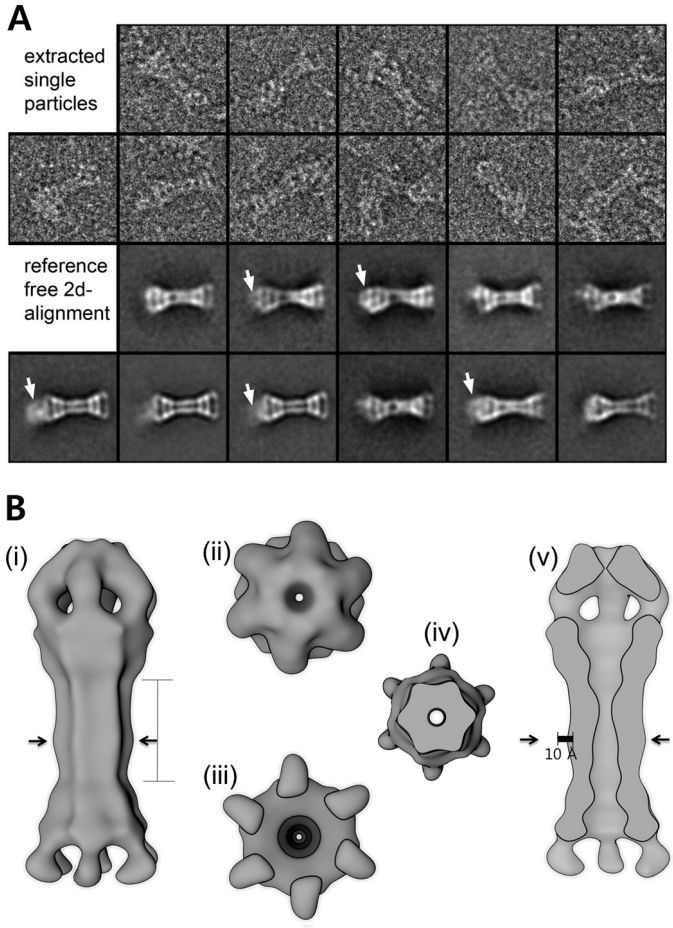


FIGURE 4. **Electron microscopic analysis of the binding interface between MexA and OprM.** *A*, representative single particles of *A. actinomycetemcomitans* MacA-MexA$\alpha$ hybrid and *A. actinomycetemcomitans* MacA-OprM$\alpha$ hybrid dimer, preserved in negative stain (uranyl-formate) and imaged at 80,000× magnification. Reference-free class averages reveal flexibility in one of the two ends (*arrows*), whereas the other end is stable. *B*, surface representations of the reconstructed density map from electron microscope images, displayed in a side (*i*), top (*ii*), bottom (*iii*), horizontal section (*iv*), and vertical section views (*v*). The central barrel and its bulge are indicated by a *line* and *arrows*. The 10-Å *scale bar* is shown, indicating that the length of the bulge is ~3 Å. *2d*, two-dimensional.

the cogwheel in the OprM $\alpha$-barrel and the concave face of the cogwheel in the MexA $\alpha$-barrels (Fig. 5*C*). The guanidinium group of the arginine residue formed a hydrogen bond with the backbone carbonyl group of the $\alpha$-barrel tip region of OprM. The hydroxyl group of Ser-130 in MexA formed a hydrogen bond with OprM Ser-198 (or Asn-410 in repeat 2). The most striking interaction was mediated by Leu-123, which is most conserved among MFPs. All the OEPs, including TolC, OprM, and CusC, had a conserved motif at the $\alpha$-barrel tip region, Val/Thr-Gly-Val, which made a characteristic sharp bend and rendered Val/Thr and Val residues facing in the same direction. The Leu-123 residue of MexA, together with Leu-122, created a hydrophobic interaction with Val-201 in repeat 1 (or Val-408 in repeat 2) of OprM, as observed in the hydrophobic interaction between the helices in the coiled-coil structure. These interactions, mediated by the three conserved residues, are all preserved in the complex models of AcrA-TolC and MacA-TolC (Fig. 5*E*). Additionally, 18 polar interactions were found between MexA and OprM (supplemental Table S2). For instance, Asp-126 of MexA formed a salt bridge with Arg-190 of OprM repeat 1 or Lys-402 of OprM repeat 2.

*TolC and AcrA Affinity to Peptidoglycan from E. coli*—In Gram-negative bacteria, a peptidoglycan layer transverses the periplasmic space where OEP and MFP interact *in vivo*. It has been reported that a periplasmic domain of TdeA, a TolC homolog, has an intrinsic affinity to peptidoglycan (48). For these reasons, we examined whether or not the purified proteins of the full-length TolC and AcrA interact with peptidoglycan from *E. coli*. We used peptidoglycan from the Gram-positive bacteria *Staphylococcus aureus* as a negative control. The results indicated that TolC and AcrA co-precipitated with peptidoglycan from *E. coli* but not with that from *S. aureus* (Fig. 6). These observations indicated that both TolC and AcrA proteins have a specific affinity toward *E. coli* peptidoglycan. We also observed that the amounts of TolC and AcrA that co-precipitated increased by co-incubation of the two proteins with the *E. coli* peptidoglycan (Fig. 6). Our findings further suggested that the binding affinity of TolC to AcrA was promoted by peptidoglycan.

## DISCUSSION

In the crystal structures of TolC, permuted salt bridges or hydrogen bonds between the neighboring protomers kept the channel closed (6, 7). When the interaction was disrupted, the TolC channel partially opened spontaneously (7). Similar interactions were also found in the crystal structure of OprM in the closed state, demonstrating 12 polar interactions (46). However, the number of intermolecular interactions associated with channel closing was less than the putative interactions for the association of OprM with MexA residues. Considering the conserved leucine residue-mediated hydrophobic interaction at the six binding interfaces, the intermolecular binding energy should have overcome the interhelical channel closing energy. This finding indicates OprM binding to MexA is more thermodynamically favorable than OprM channel closing.

To allow OprM to efficiently and rapidly bind MexA, hexamerization of MexA is required to expose the six-bladed cogwheel at the $\alpha$-hairpin tip region. We observed that the monomeric form of MexA or AcrA did not interact strongly with the OprM or TolC $\alpha$-barrel tip regions in the hexameric form (14), whereas the hexamerized form of MexA $\alpha$-hairpin domains demonstrated a strong affinity to OprM. The homohexamerization of MexA could be achieved by interaction with MexB. As observed in the case of CusB binding to CusA (19), the RND-type inner membrane transporter provided the platform for the hexamerization of MFP. This mechanism implies that only MexB-bound MexA can bind to OprM, which prevents channel opening of the OEP by MFPs alone. In addition to the synergistic interaction with MexB, the interaction with OprM can also contribute to the hexamerization of MexA. It was observed previously that hexamerization of *E. coli* MacA and AcrA proteins was induced by the TolC tip-containing protein (14, 31). These observations were consistent with the change in proteolytic sensitivity of the membrane proximal domain of MFPs by the OEP (16, 49, 50), which may stem from the global conformational change induced by the hexamerization of MFPs, in particular the mobile membrane proximal domains.

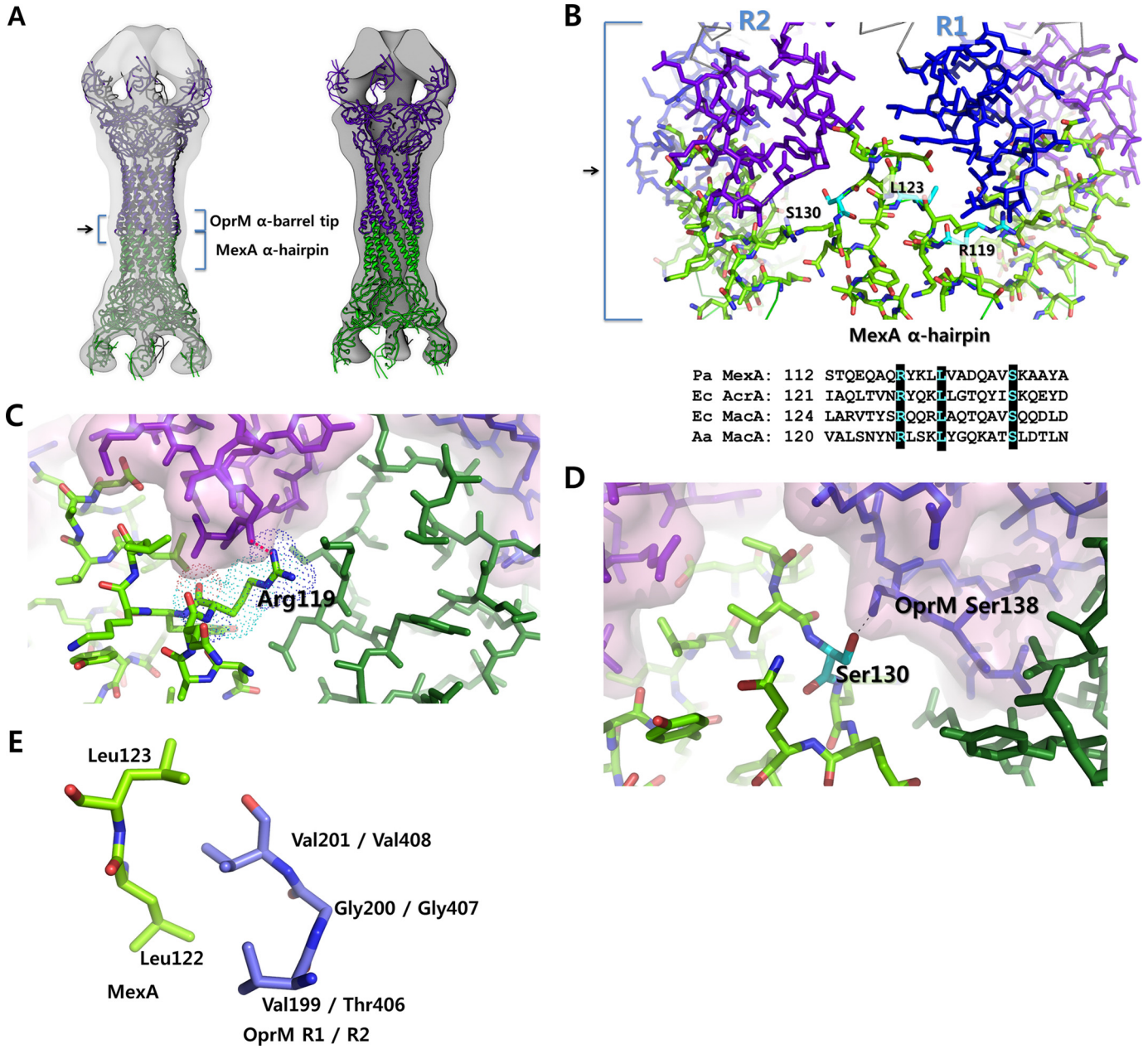


FIGURE 5. **Modeled structures for MexA α-hairpin and OprM α-barrel tip regions, docked to the electron density map.** *A*, the hexameric structure of *A. actinomycetemcomitans* MacA-MexAα hybrid (shown in *green*) and the hexameric model of *A. actinomycetemcomitans* MacA-OprMα hybrid dimer (shown in *violet*) were fitted to the electron density map. The MexA α-hairpin and OprM α-barrel tip regions are indicated. The *arrow* indicates the bulged region in the electron density map whose shape matches well with the location of the binding interface between MexA α-hairpin and OprM α-barrel tip regions. *B*, stick representations at the interface between MexA α-hairpin (shown in *green*) and OprM α-barrel tip region (shown in *blue* for repeat 1 and *violet* for repeat 2). The conserved amino acid residues, Arg-119, Leu-123, and Ser-130 of MexA are shown as *cyan*. The *bottom panel* shows a sequence alignment on the α-hairpin tip region of *P. aeruginosa* (*Pa*) MexA, *E. coli* (*Ec*) AcrA, *E. coli* MacA, and *A. actinomycetemcomitans* MacA where the key conserved amino acid residues Arg, Leu, and Ser are highlighted. *C*, close-up view of MexA Arg-119-mediated interactions. The van der Waals radius of MexA Arg-119 is displayed using dots. The *red dotted line* indicates hydrogen bonding between the guanidine group of MexA Arg-119 and the OprM backbone carbonyl group. The OprM tip regions are shown as *violet* or *blue* and covered by a semitransparent surface representation. The MexA residues are colored *green* or *dark green*. The long aliphatic chain of Arg-119 occupies the space between the two proteins, and the terminal group makes a polar interaction. *D*, a close-up view of MexA Ser-130-mediated interaction. MexA Ser-130 makes a hydrogen bond with OprM Ser-138 in repeat 1 and with OprM Asn-410 in repeat 2 (not shown). *E*, a close-up view of MexA Leu-123-mediated interactions. The conserved Leu-123 and Leu-122 residues make a leucine-zipper-like interaction with the OprM (V/T)GV motif in both repeats 1 and 2.

There remains an obstacle for MexA to bind rapidly to OprM even though the binding reaction may be thermodynamically favorable. In our binding model, the residues for the channel closing are mostly involved indirectly in the binding to MFP. Consistent to the model, the TolC mutant generated by disruption of the hydrogen bonding network in channel closing were functional *in vivo*, suggesting that the residues involved in channel closing do not play essential roles in MFP binding (7). Thus, it is unlikely that the MexA residues directly induce the channel opening of OprM. If this is the case, what interaction would result in the opening the OEP channel? We note that thermal motion associated with the α-hairpins of the OEP

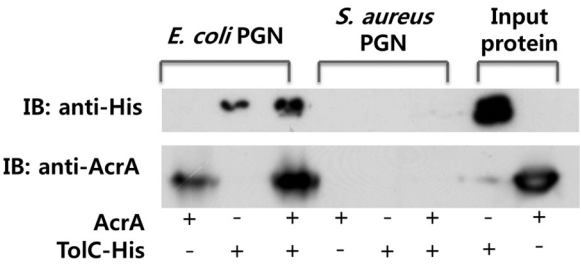


FIGURE 6. **The synergistic binding of AcrA and TolC to *E. coli* peptidoglycan.** The full-length AcrA, except for the signal peptide and lipid modification (AcrA; 80 $\mu$g) and/or the full-length TolC with the C-terminally hexahistidine tag (TolC-His; 70 $\mu$g) were incubated with the purified peptidoglycans (*PGN*; 200 $\mu$g) from *E. coli* or *S. aureus* in an insoluble form. After washing with PBS, the peptidoglycans were applied to SDS-PAGE and analyzed by Western blot with the indicating antibodies.

could break the interhelical interactions responsible for channel closing and thus induce occasional partial channel opening. At the moment of thermally induced opening, the MexA $\alpha$-hairpin tip region could make the necessary interaction with the OprM $\alpha$-barrel tip region to induce full opening of the OprM channel by cooperative binding. It is noteworthy that the OEPs and MFPs are found to be associated in the *in vivo* environment. In this study, we observed partial affinities of TolC and AcrA to peptidoglycan, but also a synergistic binding of peptidoglycan to AcrA with TolC. This observation tempts us to speculate that peptidoglycan may be a candidate for increasing the likelihood of collision between OEPs and MFPs, which in turn facilitates capture of the open state of OEP by MFP.

Aside from our observations, other cross-linking experiments have implied that the MFP tip region is associated with the outside of the $\alpha$-barrel of the OEP (11, 12, 51–54). Based on these results, several assembly models have been proposed and are generally accepted in this field (11, 16, 55). Janganan *et al.* (52) reported recently that the channel opening of the outer membrane protein channel is induced by interaction with the membrane fusion protein MtrC in the *Neisseria gonorrhoeae* MtrCDE pump. However, these studies cannot exclude the possibility that the models based on interactions between MFP and OEP may represent an intermediate or transient state of the assembly because the cross-linking experiments could capture both transient and intermediate states. Besides, the results from the cross-linking experiments were not supported by genetic data as the mutant genes used for the experiments were not as functional as wild type genes (13, 14). In contrast, the crystallographic and electron microscopic tools used in this study provide structural information for the stable complexes, and our results were supported coordinately with biochemical and genetic data (13, 14, 29–31). Therefore, although the interaction between MFP and the outside of the $\alpha$-barrel of OEP may contribute to partial opening of the channel at an intermediate stage during the assembly, it is more likely that MFP makes a stable interaction with the tip region of OEP as described in this study.

The assembly and channel-opening mechanisms in the multidrug efflux pump are considered an important issue. This study detailed the adapter bridging model by illustrating the cogwheel-to-cogwheel interaction between MFP and OEP by use of crystal structure and electron microscope images. Owing to the atomic model for the complex, we make a reasonable explanation as to the mechanism for binding interaction between MFP and OEP. Although the exact mechanism must await confirmation through elucidation of additional ternary complex crystal structures, this study provides a better understanding of the underlying tripartite drug efflux pumps mechanisms that play an important role in the incidence of multidrug resistance in Gram-negative bacteria.

*Acknowledgments—We thank Pohang Accelerator Laboratory (Pohang, Korea) for help with data processing. Electron microscopy imaging was performed at the National Resource for Automated Molecular Microscopy, which was supported by the National Institutes of Health though the National Center for Research Resources P41 Program RR17573.*

## REFERENCES

1. Putman, M., van Veen, H. W., and Konings, W. N. (2000) Molecular properties of bacterial multidrug transporters. *Microbiol. Mol. Biol. Rev.* **64,** 672–693
2. Zgurskaya, H. I., and Nikaido, H. (2000) Multidrug resistance mechanisms: Drug efflux across two membranes. *Mol. Microbiol.* **37,** 219–225
3. Morshed, S. R., Lei, Y., Yoneyama, H., and Nakae, T. (1995) Expression of genes associated with antibiotic extrusion in *Pseudomonas aeruginosa*. *Biochem. Biophys. Res. Commun.* **210,** 356–362
4. Lewis, K. (2000) Translocases: A bacterial tunnel for drugs and proteins. *Curr. Biol.* **10,** R678–681
5. Murakami, S., Nakashima, R., Yamashita, E., and Yamaguchi, A. (2002) Crystal structure of bacterial multidrug efflux transporter AcrB. *Nature* **419,** 587–593
6. Koronakis, V., Sharff, A., Koronakis, E., Luisi, B., and Hughes, C. (2000) Crystal structure of the bacterial membrane protein TolC central to multidrug efflux and protein export. *Nature* **405,** 914–919
7. Bavro, V. N., Pietras, Z., Furnham, N., Pérez-Cano, L., Fernández-Recio, J., Pei, X. Y., Misra, R., and Luisi, B. (2008) Assembly and channel opening in a bacterial drug efflux machine. *Mol. Cell* **30,** 114–121
8. Touzé, T., Eswaran, J., Bokma, E., Koronakis, E., Hughes, C., and Koronakis, V. (2004) Interactions underlying assembly of the *Escherichia coli* AcrAB-TolC multidrug efflux system. *Mol. Microbiol.* **53,** 697–706
9. Husain, F., Humbard, M., and Misra, R. (2004) Interaction between the TolC and AcrA proteins of a multidrug efflux system of *Escherichia coli*. *J. Bacteriol.* **186,** 8533–8536
10. Mikolosko, J., Bobyk, K., Zgurskaya, H. I., and Ghosh, P. (2006) Conformational flexibility in the multidrug efflux system protein AcrA. *Structure* **14,** 577–587
11. Symmons, M. F., Bokma, E., Koronakis, E., Hughes, C., and Koronakis, V. (2009) The assembled structure of a complete tripartite bacterial multidrug efflux pump. *Proc. Natl. Acad. Sci. U.S.A.* **106,** 7173–7178
12. Lobedanz, S., Bokma, E., Symmons, M. F., Koronakis, E., Hughes, C., and Koronakis, V. (2007) A periplasmic coiled-coil interface underlying TolC recruitment and the assembly of bacterial drug efflux pumps. *Proc. Natl. Acad. Sci. U.S.A.* **104,** 4612–4617
13. Kim, H. M., Xu, Y., Lee, M., Piao, S., Sim, S. H., Ha, N. C., and Lee, K. (2010) Functional relationships between the AcrA hairpin tip region and the TolC aperture tip region for the formation of the bacterial tripartite efflux pump AcrAB-TolC. *J. Bacteriol.* **192,** 4498–4503
14. Xu, Y., Lee, M., Moeller, A., Song, S., Yoon, B. Y., Kim, H. M., Jun, S. Y., Lee, K., and Ha, N. C. (2011) Funnel-like hexameric assembly of the periplasmic adapter protein in the tripartite multidrug efflux pump in Gram-negative bacteria. *J. Biol. Chem.* **286,** 17910–17920
15. Reffay, M., Gambin, Y., Benabdelhak, H., Phan, G., Taulier, N., Ducruix, A., Hodges, R. S., and Urbach, W. (2009) Tracking membrane protein association in model membranes. *PloS One* **4,** e5035
16. Zgurskaya, H. I., Krishnamoorthy, G., Ntreh, A., and Lu, S. (2011) Mech-

anism and function of the outer membrane channel TolC in multidrug resistance and physiology of enterobacteria. *Front. Microbiol.* **2,** 189
17. Stegmeier, J. F., Polleichtner, G., Brandes, N., Hotz, C., and Andersen, C. (2006) Importance of the adaptor (membrane fusion) protein hairpin domain for the functionality of multidrug efflux pumps. *Biochemistry* **45,** 10303–10312
18. Janganan, T. K., Bavro, V. N., Zhang, L., Matak-Vinkovic, D., Barrera, N. P., Venien-Bryan, C., Robinson, C. V., Borges-Walmsley, M. I., and Walmsley, A. R. (2011) Evidence for the assembly of a bacterial tripartite multidrug pump with a stoichiometry of 3:6:3. *J. Biol. Chem.* **286,** 26900–26912
19. Su, C. C., Long, F., Zimmermann, M. T., Rajashankar, K. R., Jernigan, R. L., and Yu, E. W. (2011) Crystal structure of the CusBA heavy metal efflux complex of *Escherichia coli*. *Nature* **470,** 558–562
20. Li, X. Z., Nikaido, H., and Poole, K. (1995) Role of mexA-mexB-oprM in antibiotic efflux in *Pseudomonas aeruginosa*. *Antimicrob. Agents Chemother.* **39,** 1948–1953
21. Akama, H., Matsuura, T., Kashiwagi, S., Yoneyama, H., Narita, S., Tsukihara, T., Nakagawa, A., and Nakae, T. (2004) Crystal structure of the membrane fusion protein, MexA, of the multidrug transporter in *Pseudomonas aeruginosa*. *J. Biol. Chem.* **279,** 25939–25942
22. Higgins, M. K., Bokma, E., Koronakis, E., Hughes, C., and Koronakis, V. (2004) Structure of the periplasmic component of a bacterial drug efflux pump. *Proc. Natl. Acad. Sci. U.S.A.* **101,** 9994–9999
23. Trépout, S., Taveau, J. C., Benabdelhak, H., Granier, T., Ducruix, A., Frangakis, A. S., and Lambert, O. (2010) Structure of reconstituted bacterial membrane efflux pump by cryo-electron tomography. *Biochim. Biophys. Acta* **1798,** 1953–1960
24. Trépout, S., Taveau, J. C., Mornet, S., Benabdelhak, H., Ducruix, A., and Lambert, O. (2007) Organization of reconstituted lipoprotein MexA onto supported lipid membrane. *Eur. Biophys. J.* **36,** 1029–1037
25. Kobayashi, N., Nishino, K., and Yamaguchi, A. (2001) Novel macrolide-specific ABC-type efflux transporter in *Escherichia coli*. *J. Bacteriol.* **183,** 5639–5644
26. Yamanaka, H., Kobayashi, H., Takahashi, E., and Okamoto, K. (2008) MacAB is involved in the secretion of *Escherichia coli* heat-stable enterotoxin II. *J. Bacteriol.* **190,** 7693–7698
27. Lin, H. T., Bavro, V. N., Barrera, N. P., Frankish, H. M., Velamakanni, S., van Veen, H. W., Robinson, C. V., Borges-Walmsley, M. I., and Walmsley, A. R. (2009) MacB ABC transporter is a dimer whose ATPase activity and macrolide-binding capacity are regulated by the membrane fusion protein MacA. *J. Biol. Chem.* **284,** 1145–1154
28. Xu, Y., Sim, S. H., Nam, K. H., Jin, X. L., Kim, H. M., Hwang, K. Y., Lee, K., and Ha, N. C. (2009) Crystal structure of the periplasmic region of MacB, a noncanonic ABC transporter. *Biochemistry* **48,** 5218–5225
29. Yum, S., Xu, Y., Piao, S., Sim, S. H., Kim, H. M., Jo, W. S., Kim, K. J., Kweon, H. S., Jeong, M. H., Jeon, H., Lee, K., and Ha, N. C. (2009) Crystal structure of the periplasmic component of a tripartite macrolide-specific efflux pump. *J. Mol. Biol.* **387,** 1286–1297
30. Xu, Y., Sim, S. H., Song, S., Piao, S., Kim, H. M., Jin, X. L., Lee, K., and Ha, N. C. (2010) The tip region of the MacA $\alpha$-hairpin is important for the binding to TolC to the *Escherichia coli* MacAB-TolC pump. *Biochem. Biophys. Res. Commun.* **394,** 962–965
31. Xu, Y., Song, S., Moeller, A., Kim, N., Piao, S., Sim, S. H., Kang, M., Yu, W., Cho, H. S., Chang, I., Lee, K., and Ha, N. C. (2011) Functional implications of an intermeshing cogwheel-like interaction between TolC and MacA in the action of macrolide-specific efflux pump MacAB-TolC. *J. Biol. Chem.* **286,** 13541–13549
32. Suloway, C., Pulokas, J., Fellmann, D., Cheng, A., Guerra, F., Quispe, J., Stagg, S., Potter, C. S., and Carragher, B. (2005) Automated molecular microscopy: The new Leginon system. *J. Struct. Biol.* **151,** 41–60
33. Lander, G. C., Stagg, S. M., Voss, N. R., Cheng, A., Fellmann, D., Pulokas, J., Yoshioka, C., Irving, C., Mulder, A., Lau, P. W., Lyumkis, D., Potter, C. S., and Carragher, B. (2009) Appion: An integrated, database-driven pipeline to facilitate EM image processing. *J. Struct. Biol.* **166,** 95–102
34. Roseman, A. M. (2003) Particle finding in electron micrographs using a fast local correlation algorithm. *Ultramicroscopy* **94,** 225–236
35. Scheres, S. H., Valle, M., Nuñez, R., Sorzano, C. O., Marabini, R., Herman, G. T., and Carazo, J. M. (2005) Maximum likelihood multireference refinement for electron microscopy images. *J. Mol. Biol.* **348,** 139–149
36. Sorzano, C. O., Marabini, R., Velázquez-Muriel, J., Bilbao-Castro, J. R., Scheres, S. H., Carazo, J. M., and Pascual-Montano, A. (2004) XMIPP: A new generation of an open-source image processing package for electron microscopy. *J. Struct. Biol.* **148,** 194–204
37. Goddard, T. D., Huang, C. C., and Ferrin, T. E. (2007) Visualizing density maps with UCSF Chimera. *J. Struct. Biol.* **157,** 281–287
38. Otwinosky, Z., and Minor, W. (1997) Processing of X-ray diffraction data collected in oscillation mode. *Methods in Enzymology*, Vol. 276, *Macromolecular Crystallography, part A*. Academic Press, NY
39. Collaborative Computational Project, Number 4 (1994) The CCP4 suite: Programs for protein crystallography. *Acta Crystallogr. D Biol. Crystallogr.* **50,** 760–763
40. Emsley, P., and Cowtan, K. (2004) Coot: Model-building tools for molecular graphics. *Acta Crystallogr. D Biol. Crystallogr.* **60,** 2126–2132
41. Adams, P. D., Grosse-Kunstleve, R. W., Hung, L. W., Ioerger, T. R., McCoy, A. J., Moriarty, N. W., Read, R. J., Sacchettini, J. C., Sauter, N. K., and Terwilliger, T. C. (2002) PHENIX: Building new software for automated crystallographic structure determination. *Acta Crystallogr. D Biol. Crystallogr.* **58,** 1948–1954
42. DeLano, W. L. (2010) *The PyMOL Molecular Graphics System*, version 1.3r1, Schrödinger, LLC, New York
43. Piao, S., Xu, Y., and Ha, N. C. (2008) Crystallization and preliminary x-ray crystallographic analysis of MacA from *Actinobacillus actinomycetemcomitans*. *Acta Crystallogr. Sect. F Struct. Biol. Cryst. Commun.* **64,** 391–393
44. Leduc, M., Fréhel, C., Siegel, E., and Van Heijenoort, J. (1989) Multilayered distribution of peptidoglycan in the periplasmic space of *Escherichia coli*. *J. Gen. Microbiol.* **135,** 1243–1254
45. Marcyjaniak, M., Odintsov, S. G., Sabala, I., and Bochtler, M. (2004) Peptidoglycan amidase MepA is a LAS metallopeptidase. *J. Biol. Chem.* **279,** 43982–43989
46. Akama, H., Kanemaki, M., Yoshimura, M., Tsukihara, T., Kashiwagi, T., Yoneyama, H., Narita, S., Nakagawa, A., and Nakae, T. (2004) Crystal structure of the drug discharge outer membrane protein, OprM, of *Pseudomonas aeruginosa*: Dual modes of membrane anchoring and occluded cavity end. *J. Biol. Chem.* **279,** 52816–52819
47. Brünger, A. T., Adams, P. D., Clore, G. M., DeLano, W. L., Gros, P., Grosse-Kunstleve, R. W., Jiang, J. S., Kuszewski, J., Nilges, M., Pannu, N. S., Read, R. J., Rice, L. M., Simonson, T., and Warren, G. L. (1998) Crystallography and NMR system: A new software suite for macromolecular structure determination. *Acta Crystallogr. D Biol. Crystallogr.* **54,** 905–921
48. Kim, S., Yum, S., Jo, W. S., Lee, B. L., Jeong, M. H., and Ha, N. C. (2008) Expression and biochemical characterization of the periplasmic domain of bacterial outer membrane porin TdeA. *J. Microbiol. Biotechnol.* **18,** 845–851
49. Modali, S. D., and Zgurskaya, H. I. (2011) The periplasmic membrane proximal domain of MacA acts as a switch in stimulation of ATP hydrolysis by MacB transporter. *Mol. Microbiol.* **81,** 937–951
50. Ge, Q., Yamada, Y., and Zgurskaya, H. (2009) The C-terminal domain of AcrA is essential for the assembly and function of the multidrug efflux pump AcrAB-TolC. *J. Bacteriol.* **191,** 4365–4371
51. Tamura, N., Murakami, S., Oyama, Y., Ishiguro, M., and Yamaguchi, A. (2005) Direct interaction of multidrug efflux transporter AcrB and outer membrane channel TolC detected via site-directed disulfide cross-linking. *Biochemistry* **44,** 11115–11121
52. Janganan, T. K., Zhang, L., Bavro, V. N., Matak-Vinkovic, D., Barrera, N. P., Burton, M. F., Steel, P. G., Robinson, C. V., Borges-Walmsley, M. I., and Walmsley, A. R. (2011) Opening of the outer membrane protein channel in tripartite efflux pumps is induced by interaction with the membrane fusion partner. *J. Biol. Chem.* **286,** 5484–5493
53. Tikhonova, E. B., Yamada, Y., and Zgurskaya, H. I. (2011) Sequential mechanism of assembly of multidrug efflux pump AcrAB-TolC. *Chem. Biol.* **18,** 454–463
54. Li, X. Z., and Nikaido, H. (2009) Efflux-mediated drug resistance in bacteria: An update. *Drugs* **69,** 1555–1623
55. Eswaran, J., Koronakis, E., Higgins, M. K., Hughes, C., and Koronakis, V. (2004) Three's company: Component structures bring a closer view of tripartite drug efflux pumps. *Curr. Opin. Struct. Biol.* **14,** 741–747

# Assembly and Channel Opening of Outer Membrane Protein in Tripartite Drug Efflux Pumps of Gram-negative Bacteria

Yongbin Xu, Arne Moeller, So-Young Jun, Minho Le, Bo-Young Yoon, Jin-Sik Kim, Kangseok Lee and Nam-Chul Ha

*J. Biol. Chem. 2012, 287:11740-11750.*
*doi: 10.1074/jbc.M111.329375 originally published online February 3, 2012*

---